The International Journal of Advanced Manufacturing Technology (2026) 143:4131–4148
https://doi.org/10.1007/s00170-026-17482-2

ORIGINAL ARTICLE

Ensemble modeling of surface roughness in the cryogenic LN_2 grinding process

Faruk Abedrabbo[1,3] · Sepideh Abolghasem[2] · Aitor Madariaga[3] · Aitor Aguirre-Ortuzar[3] · Raúl Fernández[3] · Pedro Arrazola[3]

Received: 17 November 2025 / Accepted: 12 January 2026 / Published online: 3 March 2026

Abstract
This research addresses the complexities inherent in grinding operations, aiming to identify the most effective process parameters and predict the behavior of the workpiece surface condition. This task is particularly challenging due to the difficulty of achieving smooth surfaces and complex, nonlinear interactions between input factors such as grinding conditions and cooling system type, and output factors such as surface roughness. These challenges are further intensified when considering additional elements, such as grinding wheel wear and advanced cryogenic lubricants or coolants. To address these issues, this study advances beyond traditional modeling methods, such as General Linear Regression or Random Forest models, to explore novel distributional modeling techniques, including General Additive Models for Shape and Scale and Distributional Random Forest. These advanced models are designed to elucidate the intricate connections between input factors and their corresponding outputs, mainly focusing on predicting the distribution of surface roughness profiles. The enhanced accuracy of these models (predictive error decreasing at around 7% and 24%) is instrumental in determining the most effective process parameters. These models offer deeper insights into the interdependencies in grinding operations, enabling more precise process control. Additionally, these models shed light on the potential improvements in surface profile quality achieved by implementing cryogenic techniques, opening new paths for optimization in grinding operations.

Keywords Cryogenic grinding · Surface roughness profile · Distributional modeling

1 Background

The increasing demand for mechanical components in the automotive and aerospace sectors, combined with the strict requirements for final surface quality, and the necessity to create eco-friendly machining processes, requires effective modeling and controlling/predicting processes. In recent years, several studies investigating the replacement of pollutant fluids with cryogenic approaches in machine tools have appeared in the literature [1, 2]. This research line creates potential opportunities to reduce global warming. These studies conclude that the positive effect of cryocooling on surface quality depends on the machining conditions. Therefore, finding suitable process working windows is crucial to applying these environmental technologies in machining production lines. In this context, a new paradigm has emerged that leverages advances in Artificial Intelligence (AI) to improve in-plant decision-making and identify suitable machining conditions.

✉ Faruk Abedrabbo
anabedrabboha@uide.edu.ec

Sepideh Abolghasem
sepideh.abolghasem@csun.edu

Aitor Madariaga
amadariaga@mondragon.edu

Aitor Aguirre-Ortuzar
aaguirre@mondragon.edu

Raúl Fernández
rfernandez@mondragon.edu

Pedro Arrazola
pjarrazola@mondragon.edu

[1] International University of Ecuador (UIDE), Quito 170411, Ecuador

[2] Department of Manufacturing Systems Engineering and Management, California State University, Northridge, 18111 Nordhoff St, Northridge, CA 91330, USA

[3] Faculty of Engineering, Mondragon Unibertsitatea, Loramendi 4, Arrasate-Mondragón 20500, Spain

In the context of machining operations, grinding is one of the most prevalent finishing techniques used to achieve the desired smooth surfaces in mechanical components. The widespread adoption of grinding is due to its remarkable capability to yield high-precision dimensions and impeccable surface quality, both essential attributes in diverse applications, including but not limited to aerospace, defense, and automobiles [3]. Given the broad applicability and significance of grinding, this paper is dedicated to delving into the intricacies of this particular finishing operation. More specifically, this work uses AI tools to study the surface of ground components.

1.1 Cryogenic in grinding operations

Cryogenic cooling is a novel solution based on liquid nitrogen (LN_2) as an environmental fluid to refrigerate machining operations. Since the grinding process is a type of machining operation, it is not an exception to applying this technology. Cryogenic grinding strategies have been researched for several years. The first approach appeared in literature in 1985 [4], followed by other publications around the nineties [5, 6]. In these works, several plates of different steels were tested under the cryogenic approach using liquid nitrogen LN_2, concluding that the materials present similar surface integrity (surface roughness, microstructure alterations, and residual stresses) compared to the conventional flood pollutant cooling system. Even for certain grinding conditions, materials present significant improvements in surface integrity.

Literature also includes studies on the cryogenic grinding process for plates and shafts on different materials (AISI 316, AISI 1020, and MS1), to evaluate forces [7, 8], energy consumption [8], and fatigue [9]. In our previous work, the use of LN_2 in conjunction with a minimum quantity of lubrication (MQL) as a cooling/lubricant system was analyzed in the grinding process of shafts [2]. These pioneering studies have demonstrated that cryogenic grinding can be an eco-friendly alternative to conventional flood grinding (WET). However, there is still a lack of a quantitative relationship between process conditions, surface integrity, and in-service performance. This relationship is significant when defining process conditions of components subjected to fatigue.

1.2 Artificial intelligence in machining

AI is a vast field because it can be applied in a wide range of industrial applications. In the case of AI for machining operations, the literature can be classified into two prominent groups. Both groups focus on predicting response variables, such as machining forces or properties of the machined surface (defined as surface integrity). The first group is based on fuzzy logic (FL) and genetic algorithms (GA), which are heuristics derived from expert human knowledge, capable of optimizing a response variable of interest in the studied problem. The second group uses machine learning (ML) techniques based on data to replace the lack of knowledge or expertise related to a process. In this context, ML models predict process outcomes and analyze interactions between input and output factors without recreating the complete problem or expanding the experimental procedure.

1.2.1 Machine learning

The vast majority of ML techniques in machining operations have focused on Artificial Neural Networks (ANN) to predict surface integrity, eliminating the need for expensive and time-consuming characterization tests. The first studies implementing ANN in machining research appeared in the nineties [10, 11]. The most common parameter to predict has been mean surface roughness [12–16]. However, over time, other parameters have been mapped and predicted, such as drilling torque [17], energy consumption [18], material removal rate [19], and remaining useful life. tool life [20], machining-induced maximum principal residual stresses [21], fatigue strength [22], and fatigue crack propagation of machined component [23, 24].

While ANN stands out as the most extensively employed ML technique in machining for reasonably accurately predicting process parameters and properties of machined components, noteworthy limitations pertain to their interpretability and explainability. Consequently, ANN are commonly characterized as “black-box” function approximators [25]. Further compounding these challenges are tendencies towards high bias and susceptibility to overfitting [26]. To mitigate these drawbacks, recent studies have introduced more sophisticated ML methodologies. Notable among these are General Linear Regression (GLM) [27, 28], Support Vector Machine (SVM) [29, 30], ensemble models such as Random Rorest (RF) [31, 32]. The strategic application of these models within machining operations enhances the interoperability of these variables, albeit with certain limitations.

For example, GLM support complete explainability; however, these models are not flexible enough to obtain good accuracy of complex phenomena such as machining operations, in which interaction between variables is intrinsically nonlinear [30]. Contrariwise, SVM, RF, or Deep Learning (DL) models are robust algorithms that significantly improve prediction accuracy. Although models based on SVM and, especially, DL models can capture non-linear relationships, they are black boxes regarding explainability usually require big datasets to be trained on. In contrast, Random Forest models are capable of capturing non-linear

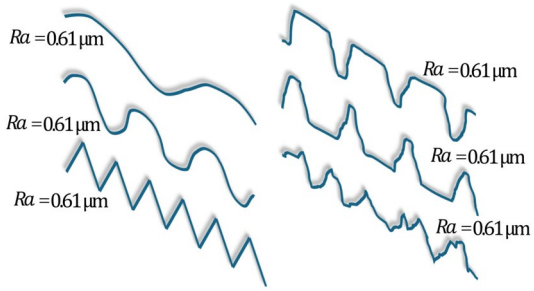

Fig. 1 Different surface roughness profiles with the same *Ra*. Adapted from [36]

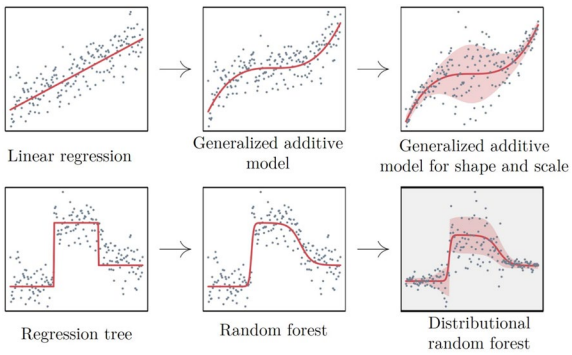

Fig. 2 Advances in modeling for predicting shape and scale distributional parameters. Adapted from [39]

relationships between input and output variables without the need for extensive datasets to be trained on, while maintaining explainability, unlike SVM or Deep Neural Networks.

The use of SVM has become more popular over the years. In some cases, this technique is used as a regression to predict certain values, such as material removal rate [30], machining forces [33], and power [29, 33]. In other cases, this technique is used as a classifier to detect a specific condition of the machining process, e.g., determine in a boring process if chatter exists or not [34], in a grinding process if the wheel is worn or not [35], or if a ground surface is burnt [32].

As the previous paragraph describes, a wide variety of response variables are reported in the literature for SVM and RF models, whereas ANN models are more focused on predicting surface roughness. This variety demonstrates the viability of applying sophisticated ML techniques to any machining process to predict material and process characteristics. This advantage is achieved because ML techniques are based on data and correlations rather than physical relationships involved in the studied problem. This versatility is why ML models have gained popularity in various manufacturing processes.

1.3 Literature gaps

Summarizing the literature review of AI approaches, there is an evident tendency to predict surface quality more than other parameters. Both ML and FL have been implemented to predict mean surface roughness as a principal variable of interest. Notwithstanding the good results achieved—where AI models have successfully predicted mean surface roughness with reasonable accuracy— this predicted variable does not offer sufficient information about surface topography, limiting professionals to decide about machining processes with incomplete information, which might not be accurate.

For example, Fig. 1 shows six different surface profiles with the same mean roughness value ($Ra = 0.61$ µm). However, differences between peaks and valleys in roughness profiles may cause fatigue cracks or alterations in tribological behavior, which reduce the component's lifespan. Additionally, some researchers have demonstrated that specific valley forms might improve lubrication retention and flow [36].

Based on the characteristics discussed above, it can be concluded that surface roughness parameters play a crucial role in enhancing product quality and enabling precise in-plant decisions. However, the literature does not provide sufficient information for the complete characterization of surface roughness profiles. Therefore, further research is necessary to improve material characterization, such as predicting mean surface roughness, deviation, and/or the root mean square of peaks and valleys. Beyond this context, AI approaches can be a promising alternative to predict some of these characteristics.

ML techniques and recent advances in data science have led to the development of novel methods that can predict multiple variables simultaneously, surpassing the standard ML approaches. For example, using distributional modeling for shape and scale, [37] creates opportunities to predict statistical distribution parameters. By assuming that a surface roughness profile has a Normal, Gamma, or Weibull distribution, distributional modeling might predict the mean and variance of these profiles.

Distributional modeling is based on two strong branches: 1) improve linear regression to obtain a generalized additive model for shape and scale (GAMLSS) [38], and 2) improve regression tree and RF to obtain distributional forest models (DRF) [39]. These modeling improvements are illustrated in Fig. 2, in which the evolution of the performance in the fitting of each model can be observed.

After a rigorous state of the art review and to the best of the authors' knowledge, while some uncertainty quantification approaches have been introduced to machining operations through Bayesian Neural Networks and Gaussian Processes [16], comprehensive distributional modeling

for complete surface characterization remains unexplored in machining operations and mechanical science. The application of advanced distributional regression models could create a range of opportunities, not only to predict mean roughness values with uncertainty bounds, but to characterize the entire probability distribution of surface characteristics of the material surface, such as residual stresses, where the measuring instrument obtains distributional responses. Nonetheless, to address these gaps and improve the understanding of cryo-grinding operations, this paper compares traditional ML models and novel distributional models (GAMLSS, DRF). Using the advantages of distributional modeling, a complete surface roughness profile characterization can be obtained to understand the influence of input parameters such as machining speeds, coolant/lubricant applied, and tool performance on the material surface.

With this complete distributional characterization, it becomes possible to analyze not only prediction improvements but also predictive uncertainty patterns, risk assessment, and quality control boundaries that are not accessible through traditional point prediction or basic uncertainty quantification methods. The benefits of this distributional approach extend to understanding material behavior variability in cryogenic grinding processes, enabling more robust process optimization and quality assurance.

To obtain a robust dataset for the modeling process, an experimental study was carried out on 60 different conditions of the cryogenic grinding process (machining conditions, cooling type, and state of the grinding wheel).

2 Material and methodology

The methodology of this work is divided into two parts. The first describes the experimental procedure, including the grinding process, the surface roughness measurements, and the data treatment to obtain a clean and useful database to develop the modeling step. The second part defines the modeling strategy and details the ML techniques and the validation process to predict: 1) the distribution of peaks' heights (*Rpm*, σ.*Rpm*), 2) the distribution of valleys' heights (*Rvm*, σ.*Rvm*), and 3) the global distribution of the surface roughness profile (*Ra*, σ.*Ra*).

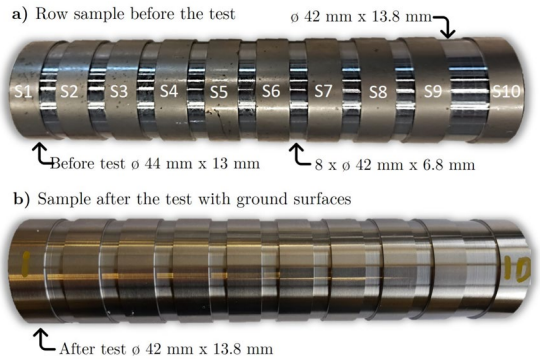

Fig. 3 Samples used in the experimentation: **a**) Pre-machined and carburized material sample, **b**) sample after the test with cryo-ground surfaces

2.1 Material and experimental set-up

The experimentation was focused on shafts made of 27MnCr5 steel, which underwent a case-hardening process to attain a martensite structure, resulting in a surface hardness ranging from 59 to 64 HRC. The carburized layer reached a depth of approximately 0.9 µm. The shaft samples, with an external diameter of 44 mm, were pre-machined to obtain straight cylinders measuring 13 mm in width. These cylinders were separated by grooves with 6.8 mm in width and 42 mm in diameter. This sample configuration allowed for the execution of 10 grinding experiments per shaft. In Fig. 3, the illustration depicts the shaft with designated surface numbers (S1 to S10) from left to right. To enhance surface identification, the S10 cylinder in the shafts was machined with a groove width of 13.8 mm (see Fig. 3).

The test consisted of producing single plunge grindings to reduce each ring diameter from 44 mm to 43.75 mm (see Fig. 3), removing a material volume of 224 mm^3 per test. Tests were done under a factorial design of experiment (DOE) 3^2, in which the tested variables were grinding wheel speed (*Vs*), and the coolant/lubricant utilized (LN_2, LN_2+MQL, and the typically WET flood solution), both variables with 3 levels. This DOE was performed twice using two workpiece speeds (*Vo*) constant during the run of each full experiment. Table 1 shows the whole information of the variables' levels.

A CBN grinding wheel of ref. 3D1V-400-15-5-25-27-B107-SA-100-V69M was used to grind the surfaces with a diameter of 400 mm and a width of 15 mm was mounted

Table 1 Levels of the factors involved in DOE

Vo [m/min]	*Vs* [m/s]	Type of coolant/lubricant system
13.82	40	WET flood solution (7.5%)
13.82	52.6	LN_2 (2 bar)
41.47	40	WET flood solution (7.5%)
41.47	63	LN_2 (2 bar) + MQL (80 ml/h)

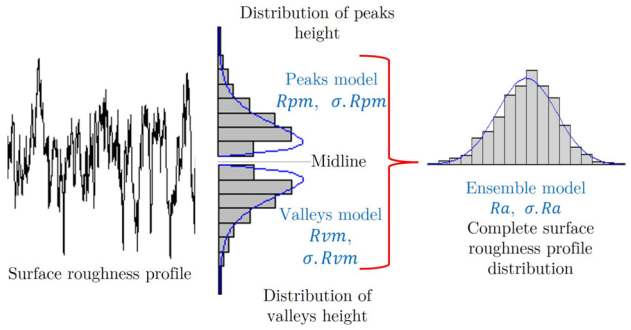

Fig. 4 Learning ensemble, graphical description for predicting surface roughness profile distribution

in the machine. The experiments were run in a commercial GER CU-1000 CNC cylindrical grinding machine, in which the specimens were clamped between centers with a grinding dog and two counterpoints. For the cryogenic grinding, the technical specifications and how this fluid was applied to the process can be found in our previous work [2].

The infeed rate in the plunge grinding process was set constant at 0.3 mm/min for all the experiments. After the plunge, a final sparkout of 10 workpiece revolutions was produced on each test. Additionally, to evaluate the effect of wheel performance (wear), the 10 cylinders were ground under the same grinding conditions consecutively, removing 2240 mm^3 (224 mm^3 per ring) without dressing the wheel. In this way, the grinding wheel performance was considered an additional variable for the process modeling. A total of 160 surfaces were machined as a result of this procedure. Between machining conditions, the grinding wheel was dressed to restart the wheel performance. The depth was 4 µm through 20 passes with a 200 mm/min transversal feed. The dressing speed changes according to the experiments, taking the same value as *Vs* in each experiment.

2.2 Data collection and modeling strategy

After the experiments, the roughness profiles of the ground surfaces were measured by the contact Mitutoyo roughness tester SJ-210, following the ISO 4287:1997 standard. The measurement had a cut-off length of 0.8 mm along a length of 4 mm. The roughness measurements were taken at a single line in the axial direction of the tested surfaces. The surface roughness profiles were extracted, generating 16000 points per surface.

After extracting the surface roughness profile for every tested sample, a database was created, grouping more than 2.5 million observations. This database was randomly split into training and testing datasets. Six surface roughness profiles, generated under different machining conditions, were excluded from both the training and validation phases. These profiles will be used later exclusively for model testing, which occurs after the model has been fully trained and optimized.

Table 2 Description of variables used in the modeling and prediction of surface roughness

Variable	Description
Vs	Numeric variable obtained from the Design of Experiments (DOE)
Vo	Numeric variable obtained from the Design of Experiments (DOE)
GroundVol	Numeric variable representing the cumulative volume ground by the grinding wheel in mm^3
LN_2	Factor variable ranging between 0 and 1
WET	Factor variable ranging between 0 and 1
LN_2+MQL	Factor variable ranging between 0 and 1
z	Numeric variable representing the height of the peak or the depth of the valley in microns

To model the roughness parameters of the ground surfaces, a novel approach was employed consisting of an ensemble learning of several ML models. This strategy consisted of dividing roughness profile peaks and valleys by the mean line, as seen in Fig. 4. In this way, the model can be developed independently, creating new opportunities to understand the influence of input parameters on surface roughness. In fact, the geometry of the valleys, which act as micronotch, and therefore stress raiser, is critical to asses the fatigue performance of machined components [40]. In addition, this ensemble model helps predict the mean surface roughness and global dispersion of the surface profile, allowing a more realistic approximation, as seen in Fig. 4.

After separating the peaks and valleys observations, the valley data set was transformed by applying the absolute value of the observation to obtain only positive values. Then, on peaks and valleys data sets, the points of surface roughness with a zero value were deleted from the data since these values do not influence the roughness profile. However, with only positive values, several statistical distributions from (<0 to inf) are practical to fit, expanding the possibilities to model the surface roughness distribution. For example, Gamma, log normal, or truncated normal distribution can be suitable distributions to be fixed in the phenomena.

Finally, two training datasets were obtained for peaks and valleys, with around 1.1 million observations for each one. Both datasets had the seven variables described in Table 2. The testing dataset had the same variables as the training dataset but with around 100 thousand observations, including peaks and valleys information. With all these datasets, models were developed and validated using the software R to predict the distribution of peaks' heights (*Rpm*, σ.*Rpm*), the distribution of valleys' heights (*Rvm*, σ.*Rvm*), and the global distribution of the surface roughness profile (*Ra*, σ.*Ra*).

2.3 Modeling methodology

This work developed four ML models (linear model, general linear model, general additive model for shape and scale, and distributional random forest) to predict three essential distributions in the surface roughness profile of ground surfaces. These distributions explain the similarities and differences between cryogenic grinding (LN_2, LN_2+MQL) with the conventional WET grinding. The ML models developed are differentiated by their novelty and complexity. The present subsection starts by explaining the basic models. Then, continue to novel distributional models to explain the benefits, differences, and accuracy of models' evolution.

2.4 Linear modeling

Linear modeling (LM) is the most common statistical technique [31] to represent the linear correlation between two or more variables; that is why it is called the "workhorse" [41]. Commonly in ML, a predictive variable (y) can be represented through one or several predictors (x_i). The linear model for any y can be described in Eq. 1.

$$E(y|x) = \mu_i = \beta_0 + \beta_1 x_1 + \beta_2 x_2 + ... + \beta_n x_n \quad (1)$$

In Eq. 1, the predictors x_i are numerical and categorical variables, depending on the problem studied and the information taken from the phenomena. The predicted variable y is the numerical response of the predictors' weighted sum, which represents the hope or expected value μ_i in the LM. The coefficients β_i are fitted by maximum likelihood estimation (MLE), a probabilistic framework based on an optimization process to find suitable parameters.

In the case of LM, the algorithm reduces the residual sum of squares [41]. The residues or errors e_i are the differences between y predicted vs. the real value of the data. LM assumes that the errors are normally distributed. This assumption produces homoscedasticity of the errors, which means that the variance of the model is constant for all the data ranges. Also, the normality assumption produces that the model predictions are the mean values that change according to the x_i and have a constant variance. The LM approach can also be expanded by polynomial functions by aggregating to the x_i large degrees to create polynomial expressions with the form $a + bx_i + cx_i^2 + ... + dx_i^n$.

2.5 General linear models

General linear models (GLM) is the generalization of LM to expand the applications of regression models to specific statistical distributions for the response variable to explain or predict. LM works well to predict response variables with low dispersion and constant variance, like responses with Gaussian or constant distributions. However, when the response variable follows a different distribution like asymmetric, exponential, or nonparametric, the predictive performance of LM decreases since the response variable can affect the homoscedasticity of the errors, violating the normality of residuals and increasing the variance in the model.

GLM uses a link function g(.) to combine linear behavior with exponential family distributions to improve the description of the phenomena. GLM restructures the relationship between predictors and the fitted variable by linearizing the correlation using the link function g(.). This link function transforms the model to create a linear response that probably does not seem to be evident with a simple data analysis [42]. This transformation produces that the variance of each observation can be a function of its predicted value [43], creating normality and independence in the residual of the models, improving the fit and generating better predictions. The GLM can be described with Eq. 2:

$$g(E(y|x)) = \beta_0 + \beta_1 x_1 + \beta_2 x_2 + ... + \beta_n x_n \quad (2)$$

In this work, for the GLM, a Gamma distribution was applied as it effectively addresses heteroscedasticity and is well suited for continuous values, using a link function with a logarithmic transformation as follows: $g(\mu_i) = log(\mu_i)$. With this link function, the final GLM equation can be represented as shown in Eq. 3. In this equation, μ_i is the model's response, and β_i are the coefficients required to be fitted for the data. Additionally, σ_i is the standard deviation of the prediction as a function of μ_i, and a constant coefficient β_{cte} that is also fitted in the model.

$$\begin{aligned} E(y|x) \quad &= \mu_i = e^{(\beta_0+\beta_1 x_1+\beta_2 x_2+\cdots+\beta_n x_n)} \\ &\text{and} \quad \sigma_i = \beta_{\text{cte}} \cdot \mu_i \end{aligned} \quad (3)$$

2.6 General additive models for shape and scale

GLM enhances prediction performance for the response variable and models the variance as a function of the mean. However, a specific way to improve flexibility is to use general additive models for shape and scale (GAMLSS). In this strategy, the model presents the opportunity to predict parameters for shape and scale to characterize the complete distribution of the response variable. These parameters are modeled independently. Therefore, the mean and variance of the distribution can be explained as a function of the explanatory variables. This strategy is beneficial when the phenomenon presents heteroscedasticity or high dispersion in the response because it is possible to identify which process parameter directly affects the response dispersion.

GAMLSS support a number of distributions. For the case of the gamma distribution, the model presents two link functions g(.). One for the shape (α) and another for the scale (θ) parameter as follows: $g(\alpha_i) = log(\alpha_i)$, $g(\theta_i) = log(\theta_i)$. These parameters can be modeled, each independently, using nonparametric functions like linear, additive, or nonlinear expressions based on the β_i coefficients. The final GAMLSS model is described in Eq. 4:

$$\begin{aligned} \alpha_i &= e^{(\beta_0+\beta_1 x_1+\beta_2 x_2+\cdots+\beta_n x_n)} \\ \text{and } \theta_i &= e^{(\beta_0+\beta_1 x_1+\beta_2 x_2+\cdots+\beta_n x_n)} \end{aligned} \tag{4}$$

Using the Gamma parametrization in the GAMLSS model, $E(y|x) = \mu_i = \alpha_i$ is the mean of the prediction, and $Var(y|x) = \sigma_i^2 = \alpha_i^2 \cdot \theta_i^2$ is the variance. Therefore, the standard deviation of the prediction can be obtained as $\sigma_i = \alpha_i \cdot \theta_i$.

2.7 Distributional random forest

Trees and forest models are a completely different approach from traditionally linear regression methods, in which y_i is correlated to x_i by linear or polynomial functions. Here the model can incorporate nonlinear relationships or even interactions between the predictors.

Regression trees were created in 1984 by Breiman et al. [44]. Regression trees consist on partitioned every predictor variable x_i based on conditions that maximize the variance reduction, similar to how entropy is used in classification tasks. In that way, the observations can be classified into rectangles with a specific estimated value (typically using the mean square error). Random forest (RF) is a predictive model based on joining several individual regression trees. Each of these models fitted multiple regression trees by using different samples and feature subsets for each tree, improving variance control compared to standard bagging methods. Finally, the prediction is the mean estimation of all individual trees regression generated.

Distributional Random Forest (DRF) is an extension of the RF algorithm that enables the prediction of the distribution of the response variable, rather than just a single value. Instead of estimating the response variable's point value, DRF estimates the parameters that define the distribution. This is achieved by constructing distributional trees, where the mean and standard deviation parameters for the Gamma distribution are estimated using the log likelihood function. By maximizing the likelihood, DRF identifies the best parameters to fit the distribution in one tree. This approach is more flexible and can provide a more complete characterization of the data distribution, making DRF a powerful tool in statistical modeling and prediction. Equation 5 shows how the likelihood function is used to estimate the distribution's parameters.

$$\begin{aligned} (\mu, \sigma) &= \arg\max \sum_{i=1}^{n} l(\mu, \sigma; y_i) \\ \text{where, } \; l(\mu, \sigma; y_i) &= \log(\text{likelihood}(\mu, \sigma; y_i)) \end{aligned} \tag{5}$$

The trees are divided into nods, selecting the points in which the parameters of the distribution maximize the value of the likelihood. This process is the same as in RF, in which the difference is that the RF algorithm minimizes the mean square error. The distributional prediction in the tree is estimated by following one tree branch until the final value is predicted, and the prediction of the parameters is estimated by the model using only the observation of the branch. Then, the final prediction is generated by the mean of the prediction of all distributional trees generated. This final process is equivalent to using all the observations in the data to create the model but using the weighted weight of each observation, which can be represented as follows in Eq. 6:

$$(\mu, \sigma) = argmax \sum_{i=1}^{n} W_i^{tree} l(\mu, \sigma; y_i) \tag{6}$$

2.8 Model selection and validation

In order to develop accurate models for predicting the mean roughness of peaks (*Rpm*) and the mean roughness of valleys (*Rvm*), it was necessary to select the relevant variables and compare the different models. To achieve this, in the first step, the Akaike information criterion (AIC) [45] was used to evaluate linear models' performance and decide the set of variables to improve prediction quality. When the set of variables was selected, this same set was used to create the rest of the models.

AIC is an important metric that describes the tradeoff between bias and variance through the log-likelihood. The mathematical expression used to estimate the AIC is shown in Eq. 7. This equation also includes a penalty term to control the data overfitting, which is proportional to the number of independent variables (k). As the number of variables increases, the AIC also rises for the same log-likelihood value. Therefore, a model with the minimum AIC represents the model with the best predictive performance.

$$AIC = 2k - 2\ln(\text{maximum likelihood}) \tag{7}$$

In the second step, the models for *Rpm*, σ.*Rpm*, *Rvm*, and σ.*Rvm* were created, and then *Ra* and σ.*Ra* values were calculated by averaging the previous results. To validate the

performance of the models and the accuracy of the results, the root mean square error (RMSE) was applied to all variables. RMSE is a common metric used to measure the deviation between predicted and actual values. In other words, it tells us how far the predictions $(\hat{y_n})$ are from the real values in the data y_n. The expression for RMSE is described in Eq. 8. Finally, the models were compared using RMSE to select the ones that provide the most accurate predictions and explanations for surface roughness after the cryogenic cylindrical grinding process.

$$RMSE = \sqrt{\frac{\sum_1^n (\hat{y_n} - y_n))^2}{n}} \tag{8}$$

To avoid overfitting, all models were trained using 10-fold cross-validation except for the DRF models. Despite using a high-performance workstation for training the models, fitting the DRF models was limited by computational calculation. This issue is because DRF models involve building and evaluating a large number of decision trees, each trained on a different subset of the data. As a result, this requires a significant amount of computation, especially when dealing with large datasets. Additionally, DRF models involve fitting a probability distribution to the output variable at each leaf node, adding an extra layer of complexity to the model and further increasing the training time. However, despite these limitations, DRF models have demonstrated their ability to provide valuable insights into complex datasets and yielded accurate results. Although cross-validation was not performed, the models were still validated to ensure the reliability of the findings presented in this work.

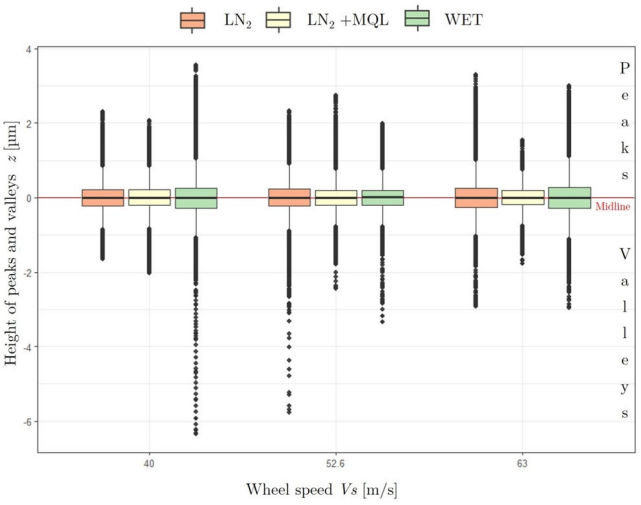

Fig. 5 Boxplot Wheel speed (*Vs*) vs height of peaks and valleys (*z*)

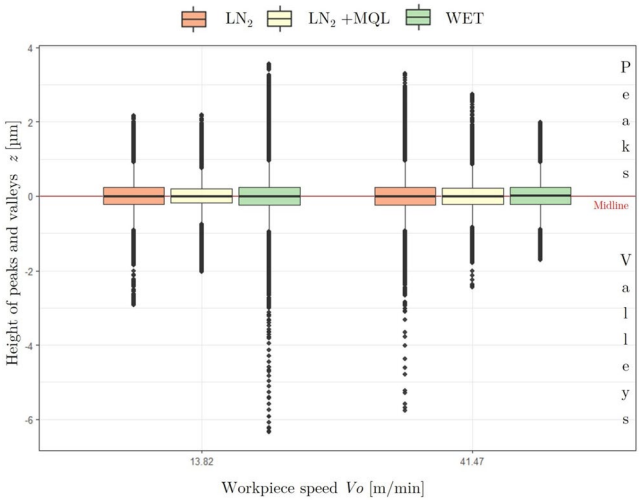

Fig. 6 Boxplot Workpiece speed (*Vo*) vs height of peaks and valleys (*z*)

3 Results and discussion

3.1 Descriptive analysis of process parameters

To analyze the effect of process parameters on surface roughness, boxplot strategies were used to find patterns or correlations between inputs and outputs. Figure 5 shows the boxplot between grinding wheel speed and the height of peaks and valleys, taking into account the three coolant liquids tested. As seen in this figure, it is possible to show that LN_2 and LN_2+MQL generally present less variance than WET. For example, for *Vs*=40 m/s in the case of LN_2 and LN_2+MQL, the height of peaks and valleys are around ±2 µm. These values are not comparable with WET, which generates a dispersion in roughness profile around 4 to -6 µm. This effect changes when the wheel speed increases. For example, for the highest speed (*Vs*=63 m/s), LN_2 presents a similar dispersion around ±3 µm as WET, but LN_2+MQL shows a considerable reduction in roughness dispersion with values around ±1.8 µm. The behavior present in this plot seems to establish a reduction in the height of peaks and valleys on the surface roughness profile as a consequence of using cryogenic liquids for cooling the grinding process.

A similar analysis was done using the workpiece speed. Figure 6 shows the height (z) of peaks and valleys for the two workpiece speeds tested. In this case, a clear tendency was found for lower speed (*Vo*=40 m/min), in which the surface roughness profile presents less dispersion for the cryogenic approaches (LN_2 and LN_2+MQL). In contrast, the WET system presents a substantial reduction in the dispersion of the surface profile for higher speed (*Vo*=63 m/min). This effect might be due to the capacity of WET coolant to refrigerate and lubricate simultaneously, a capacity that seems to be not sufficient for the LN_2 at high workpiece speed, which presents the highest variance. Another specific tendency might be that LN_2 increases surface roughness

dispersion for higher workpiece speed. This tendency seems to be totally opposite to WET, which increases dispersion for lower speeds. However, a clear highlight in this figure is that LN_2+MQL produced similar variance for both workpiece speeds, expanding the opportunity to use this approach in a complete range of cutting parameters.

To analyze the effect of the accumulative ground volume (*GroundVol*) by the wheel on the height of peaks and valleys, Fig. 7 shows the boxplot graph, in which colors clearly differentiate the three coolant systems tested. Two main highlights can be discussed in this figure. First, independently of the coolant and machining conditions, surface roughness dispersion increases as a consequence of the high accumulative ground volume of the wheel. For volumes of 1792 mm^3 and 2016 mm^3, the profile shows higher variance than for lower volumes (from 0 mm^3 to 448 mm^3). This tendency is clearly explained by the wheel dullness and wheel wear [46], in which the swarf of the material dulls the grinding wheel pores. This observation aligns with fundamental tribological principles established for similar hard steels. For instance, Wang et al. [47] demonstrated that the wear behavior of hardened 52100 steel is critically governed by the product of normal load and sliding speed (*Pv*). Their work showed that as the *Pv* value increases, friction-induced bulk surface temperatures rise significantly (exceeding $200°C$ at critical thresholds), leading to a transition from mild to severe wear [47]. Complementing this, further research by Wang et al. [48] established a direct correlation between these frictional temperature fields and wear resistance. They found that as surface temperatures rise—influenced by the material's thermal conductivity and sliding conditions—the wear resistance drops significantly due to thermal softening and microstructural changes [48]. In our grinding experiments, the accumulative ground volume represents a similar progression of mechanical and thermal loading on the wheel-workpiece interface. As the process continues, the increased interaction between the dull grains and the workpiece likely generates higher friction temperatures and altered wear mechanisms, which directly contributes to the increased dispersion of the surface roughness profile observed in Fig. 7.

Figure 8 shows the images of the state of the wheel at initial state (dressed) and after grinding 10 surfaces (2016 mm^3 material removed) for every coolant system tested. It is possible to see that the coolant which produces more dullness is the LN_2+MQL. Interestingly, this cryogenic approach also produces less surface roughness dispersion in Fig. 7. Probably, this dullness in the LN_2+MQL has a higher percentage of oil on the surface that generates a lubricant effect, producing an increase in *Ra* but with less dispersion (see the number of peaks and valleys accumulate at the ends outside the box in Fig. 7).

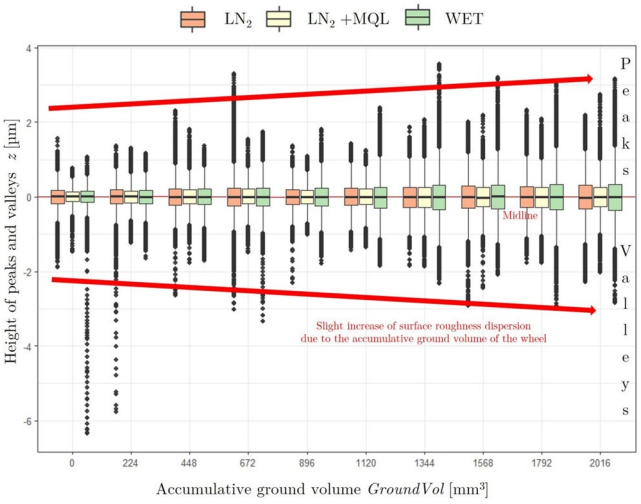

Fig. 7 Boxplot accumulative ground volume by the wheel vs height of peaks and valleys

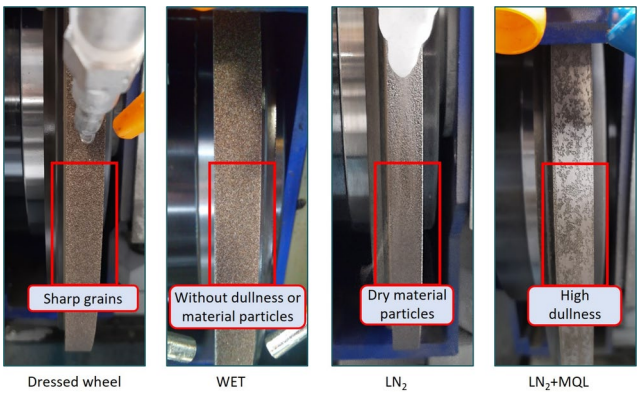

Fig. 8 Evidence of wear and dullness effect on grinding wheel

In the case of WET and LN_2, the dullness and wear of the grinding wheel seem less aggressive than LN_2+MQL, as seen in Fig. 8. This result suggests that the WET approach is the strategy that produces less dullness. This characteristic is probably achieved thanks to the flood-cooling effect that washes the wheel during grinding. However, the data analysis demonstrated that WET samples produce several points far from the surface roughness's centerline, increasing the profile's dispersion when lower speeds were applied to the process (see Fig. 7).

The color of the grinding wheel changes due to the dullness when LN_2 is used. The swarfs of the process are impregnated in the wheel because the LN_2 does not have the ability to clean the wheel. Therefore, this problem increases the *Ra* but maintains the dispersion of the profile. Figure 7 shows that dispersion is consistent despite the dullness of the grinding wheel. However, this dispersion is higher than the LN_2+MQL. Thus, the behavior suggests that LN_2 may need an external system to clean the wheel during grinding.

The second highlight in Fig. 7 is that in the first grinding experiments (*GroundVol* between 0 to 224 mm^3), WET and LN_2 produce severe dispersion on the surface roughness profile. This performance might be because the grinding wheel grains are very sharp after the dressing process, producing deep valleys on the surface. This effect coincides with the commonly known effect of grinding wheel settlement [49]. After a grinding time, the grains of the wheel begin to lose their edges, and a better surface finish is obtained. In the case of LN_2+MQL, this effect does not occur due to the highly lubricating capacity of MQL.

Although in the plots of Figs. 5, 6, and 7, you can see points outside the boxes that could initially be considered outliers in normal distribution. These points are real peaks and valleys extracted from the roughness profile. They are usually excluded from *Ra*, *Rz*, and *Rt* measurements in a conventional roughness tester due to using a Gaussian filter to smooth out irregularities and provide a more standardized roughness measure. However, this filtering process can also remove important information about the actual surface topography. For this reason, several authors might not be able to find critical differences between the surface roughness of conventional flood grinding and cryogenic grinding under the same machining conditions, especially with lower depths of cut and without grinding wheel wear [2, 8]. However, precisely, this difference between peaks and valleys scattered outside the boxes in the figures differentiate the roughness profile in the grinding processes when the cooling fluid changes. Therefore, in this study, the peaks or valleys outside the boxes will be considered valid points for both the models developed and the experimental statistical distribution.

3.2 Fitted models of LM

LM is the easiest way to analyze the influence of predictors in the response variable. For this reason, to predict surface roughness in the cylindrical plunge grinding, two LM models were developed to predict *Rpm* and *Rvm*. Then, the results of these models were computed to predict *Ra* and the global dispersion of the surface roughness profile.

Using the training dataset for peaks, a selection process was developed to find a suitable combination of machining conditions. This process was run in a sequential method with replacement, in which the process started introducing one variable in the model, and the model AIC was evaluated. Then, another variable was added to the model, and again the AIC was evaluated. This process was redundant until all variables and their squares were evaluated. The result of this process is presented in Table 3.

The model that achieved the best prediction performance in terms of AIC=83666 is a second-order regression with all the 6 variables involved in the machining process, as can be seen in Table 3. In this model, based on the best fitting, *Vs* and *GroundVol* have nonlinear behavior to predict *Rpm*. To reduce the randomness effect when dividing the training dataset, the model was also evaluated by 10-fold cross-validation, obtaining an AIC=83687. Therefore, the final LM model for *Rpm* is represented by Eq. 9. The standard deviation of the predictions estimated by the model is a constant value of $\sigma.Rpm$=0.251 µm.

$$Rpm_{LM} = 0.245 + 0.186Vs + 42.78Vs^2 + 0.002Vo + \begin{cases} -0.043\ LN_2 + MQL \\ 0\ LN_2 \\ 0.021\ WET \end{cases} + 84.30GroundVol - 7.21GroundVol^2 \quad (9)$$

As mentioned in the state of the art, predicting the dispersion of the roughness profile or its standard deviation is not common in the scientific literature. However, some authors show confidence intervals for *Ra*. For example, the authors of [50] proposed a mathematical method of predicting *Ra* and showed a confidence interval. The upper limit of this interval was 0.202 µm, which agrees with the prediction range obtained from LM for $\sigma.Rpm$.

Table 3 Sequential process to select model variables for *Rpm* in the training dataset

Model	Variables significance in the model at 95%	AIC
$Rpm = Vs$	All variables	201379
$Rpm = Vs + Vo$	All variables	201370
$Rpm = Vs + Vo + Coolant$	All variables	190003
$Rpm = Vs + Vo + Coolant + GroundVol$	All variables	110384
$Rpm = Vs + Vs^2 + Vo + Coolant + GroundVol$	All variables, except for Vs	84480
$Rpm = Vs^2 + Vo + Coolant + GroundVol$	All variables	110193
$Rpm = Vs + Vs^2 + Vo + Coolant + GroundVol + GroundVol$	**All variables, except for Vs**	**83666**
$Rpm = Vs^2 + Vo + Coolant + GroundVol + GroundVol^2$	All variables	109729
$Rpm = Vs + Vs^2 + Vo + Coolant + GroundVol^2$	All variables	97563
$Rpm = Vs^2 + Vo + Coolant + GroundVol^2$	All variables	119934
$Rpm = Vs + Vo + Coolant + GroundVol + GroundVol^2$	All variables	109910

According to Eq. 9, all machining parameters influence predicting surface roughness for peaks, and the model for valleys was directly constructed using the same variables of the peaks model. The model to predict *Rvm* is presented in Eq. 10. In this case, the model obtained a predicted performance of AIC=112020 in the 10-fold cross-validation. As the AIC suggests, the model performance of peaks is better than the model of valleys. This effect may be probably due to the higher dispersion of several valleys seen in Fig. 7. The respective standard deviation of the valleys distribution model is $\sigma.Rvm$=0.255 µm, which is similar to $\sigma.Rpm$.

$$Rvm_{LM} = 0.25 + 2.39Vs + 38.74Vs^2 + 0.002Vo + \begin{cases} -0.039\ LN_2 + MQL \\ 0\ LN_2 \\ 0.029\ WET \end{cases} + 75.76GroundVol - 6.81GroundVol^2 \quad (10)$$

Rpm_{LM} and Rvm_{LM} models show several similarities. Not only in the predictors but also in the behavior of their predictors. For example, *Vs* and *GroundVol* present the same second-order structure, producing a similar effect on surface roughness. Also, in both models, the effect of LN_2 +MQL is negative, suggesting that using LN_2+MQL can reduce the surface roughness compared to the other cooling approaches. In the case of WET and LN_2, the effects are positive with a slight difference. The contribution of WET between (0.02-0.03) can increase the surface roughness compared to the cryogenics approaches.

In the LM models, as explained in subsection 2.4, the errors of the model are normally distributed. When this assumption has been violated, the performance of the model significantly decreases because it implies that the variance is not constant in the dataset. This phenomenon is called heteroscedasticity, producing that around the zones where the variance increases, the predictions lose accuracy, increasing the prediction error. For this reason, it is vital to validate residual behavior. Figure 9a shows the quantiles behavior through a Q-Q plot for Rpm_{LM} and Fig. 9b shows the Q-Q plot for Rvm_{LM}. As seen in these figures, the assumption of Gaussian distribution is violated for both models. For this reason, LM might not be an accurate strategy for modeling *Rpm* or *Rvm*.

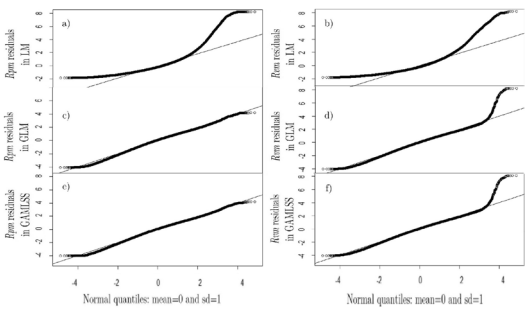

Fig. 9 Residual distribution of *Rpm* and *Rvm* in LM (**a** and **b**), GLM (**c** and **d**), and GAMLSS (**e** and **f**)

Another disadvantage of LM appears when the necessity to figure out the standard deviation of the response variable exists because LM estimates a constant variance that does not change according to the values of the predictors. The problem with a constant variance is that sometimes, it does not represent/explain the reality of the problem. As is evidenced in Figs. 5 and 6, the variance of surface roughness profiles is clearly not constant for all grinding conditions, especially for the different cooling systems tested. This behavior produces several increments/decrements in the magnitude of peaks and valleys, changing the dispersion of the surface roughness profile. Therefore, LM models are not able to predict/explain the effects of cryogenic cooling systems over conventional cooling systems that are hidden in the variance of surface roughness profile with good accuracy, which is the objective of this study.

3.3 Fitted models for GLM

As can be seen in Fig. 4, the global roughness profile follows a normal distribution. However, when the peaks and valley distribution are divided, the tendency change affects the performance of LM to predict peaks and valleys. When peaks and valleys were divided, positive distributions from 0 to R^+ were created. As shown in Fig. 4, the new response distributions fit more on Gamma distributions than on Gaussian distributions. For this reason, using GLM can improve surface roughens predictions.

Using the same variables and methodology described for the LM models, GLM models were developed for peaks and valleys. The GLM for *Rpm* and *Rvm* are presented in Eqs. 11 and 12, obtaining their values of AIC after the 10-fold cross-validation equal to -709467 and -618826, respectively.

$$log(Rpm_{GLM}) = -1.43 - 0.296Vs + 147.7Vs^2 + 0.007Vo + \begin{cases} -0.170\ LN_2 + MQL \\ 0\ LN_2 \\ 0.019\ WET \end{cases} + 300GroundVol - 50.78GroundVol^2 \quad (11)$$

$$log(Rvm_{GLM}) = -1.41 + 5.90Vs + 130.8Vs^2 + 0.007Vo + \begin{cases} -0.155\ LN_2 + MQL \\ 0\ LN_2 \\ 0.048\ WET \end{cases} + 262.1GroundVol - 40.47GroundVol^2 \quad (12)$$

In these cases, the AIC presents a negative value due to the transformation used in the models. To create the predictions assuming that the response variable follows a Gamma distribution. GLM uses a link function to predict the mean and variance in the model. For Gamma distribution, the link function is $g(\mu_i) = log(\mu_i)$. Therefore, when figuring out the AIC, the likelihood is bigger than the number of independent variables, producing a negative result. However, this behavior has not affected the AIC analysis because the

preferred model is the model with lower AIC considering the relative values. Therefore, the AICs of GLM models are lower than the AICs of the LM models, concluding that GLM can predict surface roughness better than the LM.

Additionally, the Q-Q plots of the models were plotted in Fig. 9c and d. As these graphs show, the quantiles of the residues of the GLM models present a normal distribution, diminishing the heteroscedasticity of the models. This heteroscedasticity reduction is the reason for the increment in prediction performances.

In GLM models, implementing the Gamma distribution enables the prediction of the response variable's deviation relative to the mean. This ability aids in understanding how the explanatory variable affects surface roughness dispersion. The standard deviation for the peaks model was estimated using the relation $\sigma.Rpm = e^{-0.128} \cdot Rpm$, and for the valleys model, it was estimated using the relation $\sigma.Rvm = e^{-0.116} \cdot Rvm$. By using these relations, the prediction of $\sigma.Rpm$ and $\sigma.Rvm$ becomes more accurate since they depend on the predicted values of *Rpm* and *Rvm*. Therefore, the predictions of $\sigma.Rpm$ and $\sigma.Rvm$ can vary along the GLM model, which was not possible using the LM model.

3.4 Fitted models for GAMLSS

Thanks to GLM, predicting the *Rpm*, *Rvm*, and their dispersion as a function of the mean is possible. However, $\sigma.Rpm$ and $\sigma.Rvm$ can also be modeled independently as a different set of variables from the mean. This advantage helps diminish the heteroscedasticity in the models and improve model explanation because it is possible to detect which explanatory variables affect the surface roughness dispersion more. Therefore, with the purpose of improving the predictions of surface roughness dispersion, GAMLSS models were tested under the same conditions as previous models.

Remember that in GAMLSS, the predictive variables are the parameters of the response distribution. Then, using the parametrization of the Gamma distribution, the mean and variance can be figured out. For peaks, the final models fitted after the 10-fold cross-validation are described in Eqs. 13 and 14. For this composed model, the AIC was estimated at -710900.

$$log(\alpha_{peak}) = -1.43 - 0.032Vs + 145.4Vs^2 + 0.008Vo + \begin{cases} -0.174\ LN_2 + MQL \\ 0\ LN_2 \\ 0.010\ WET \end{cases} + 298.6GroundVol - 50.20GroundVol^2 \quad (13)$$

$$log(\theta_{peak}) = -0.134 - 7.761Vs + 11.048Vs^2 + 0.0003Vo + \begin{cases} -0.010\ LN_2 + MQL \\ 0\ LN_2 \\ 0.004\ WET \end{cases} + 22.382GroundVol - 1.325GroundVol^2 \quad (14)$$

As the mean is equivalent to α_i, and the deviation is equal to $\alpha_i \cdot \theta_i$, it is possible to compare Eqs. 13 and 14 with Eq. 11, in which can be evidenced that the GAMLSS approach generates better predictive performance for *Rpm* and $\sigma.Rpm$ with a difference of 1433 points in AIC. The significant improvement in AIC is probably due to the improvement in modeling the standard deviation. Although Eq. 14 shows the same variables as Eq. 13, the coefficients are totally different.

For the model of the valleys, the behavior is similar to peaks. For shape (α_i) and scale θ_i parameters, the models achieved are described by Eqs. 15 and 16. These models show a predictive performance of -618980 in AIC. Comparing the results of Eqs. 15 and 16 with Eq. 12, GAMLSS model for valleys improves the prediction accuracy AIC in 154 points.

$$log(\alpha_{valley}) = -1.41 + 5.61Vs + 130.4Vs^2 + 0.007Vo + \begin{cases} -0.156\ LN_2 + MQL \\ 0\ LN_2 \\ 0.048\ WET \end{cases} + 261.8GroundVol - 40.35GroundVol^2 \quad (15)$$

$$log(\theta_{valley}) = -0.104 - 3.98Vs + 1.561Vs^2 - 0.0002Vo + \begin{cases} -0.0054\ LN_2 + MQL \\ 0\ LN_2 \\ 0.0046\ WET \end{cases} + 0.0046GroundVol - 0.000007GroundVol^2 \quad (16)$$

In the case of the quantile residues of the GAMLSS models. As can be noticed in Fig. 9e and f, the behavior of the residuals is almost the same as achieved in GLM models, however, by modeling the deviation of the response variable for peaks and valleys in an independent way. The improvements in prediction performance and variable explanation are considerably better for improving decision-making.

An important highlight of these models, especially in the shape parameter of the valleys model, is the significant changes in the coefficient of the variable *VolGround*. As can be noticed in Eq. 16, the coefficient of this variable is near zero. This result means that the dispersion of valleys might not be strongly affected by the wear of the grinding wheel. It probably depends more on the material and grain size of the wheel. However, the effect is contrary in the model for peaks, where the coefficient of the *VolGround* in the shape parameter is the highest of the equation. This tendency in the model might support the evidence shown in Fig. 8, in which the dullness of the grinding wheel covers the porous between the grains in the wheel, directly affecting the peaks' dispersion more.

3.5 Fitted models for DRF

The predictive performance significantly improved with the use of GAMLSS models. However, to compare and evaluate the performance of these models with a different ML approach that achieves similar distributional modeling characteristics, DRF models were also assessed.

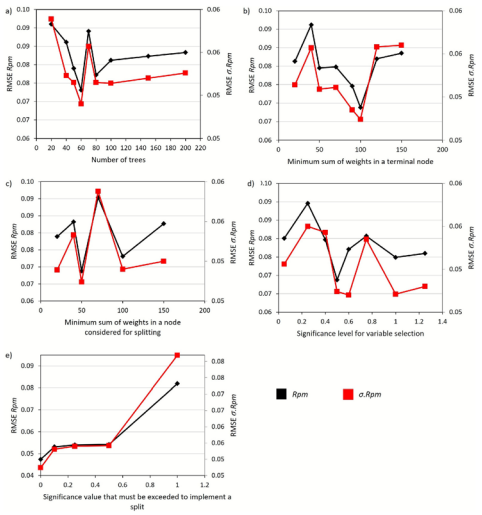

Fig. 10 Hyperparameters process optimization for DRF model for peaks. Black line represents the tendency of *Ra*, while Red line shows the tendency of $\sigma.Ra$

The DRF models were trained with all explanatory variables as it is a forest approach and does not fit polynomial expressions. All variables were considered since the previous model highlighted the significance of the machining conditions and cooling system type in predicting surface roughness. Using the same training dataset, the models were evaluated for their effectiveness in predicting *Rpm*, $\sigma.Rpm$, *Rvm*, and $\sigma.Rvm$.

Due to the fitting process of DRF models being different from GAMLSS, obtaining the AIC in these models is impossible. Therefore, DRF models were directly optimized using the RMSE for *Ra* and the global dispersion of the roughness profile $\sigma.Ra$. The optimization of the hyperparameters was done for peaks and valley models simultaneously in a sequential method. First, the process started by optimizing the number of trees (see Fig. 10a), and the rest of the parameters were fixed on a middle value. After optimizing the tree numbers, this parameter was fixed to the optimal value, and the process continued with the other parameters. The optimization process was iterative until all the parameters were estimated.

The final DRF models achieved 60 trees (see Fig. 10a). The minimum sum of weights in a node considered for splitting was 50, and the minimum sum of weights in a terminal node was optimized at 100 (see Fig. 10b and c). Additionally, the significance level for variable selection that achieved the lower RMSE was 0.5, and the minimum value to be exceeded to implement a split was $1 - pvalue = 0$ (see Fig. 10d and e). These parameters were selected in the conditions that decreased the RMSE on the test dataset for *Ra* and *Sd.Ra*. Resulting in an RMSE of 0.0688 and 0.0474, respectively.

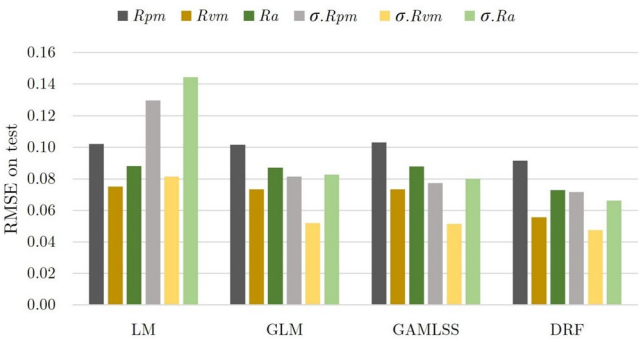

Fig. 11 RMSE on testing dataset for *Rpm*, $\sigma.Rpm$, *Rvm*, $\sigma.Rvm$, *Ra*, and $\sigma.Ra$

3.6 Models comparison and evaluation

To validate the developed ML approach on the surface roughness of ground surfaces, models were compared using RMSE for *Rpm*, $\sigma.Rpm$, *Rvm*, $\sigma.Rvm$, *Ra*, and $\sigma.Ra$ on the testing dataset. The results are shown in Fig. 11. This figure shows that LM, GLM, and GAMLSS models present strongly similar RMSE for *Rpm*, *Rvm*, and *Ra* predictions. However, the differences are clearly illustrated in the standard deviation predictions. LM estimated constant deviations that do not coincide with the naturality of surface roughness, which resulted in a considerable increase in the RMSE.

GLM and GAMLSS models decrease the RMSE in predictions of $\sigma.Rpm$, $\sigma.Rvm$ and $\sigma.Ra$. This performance is achieved thanks to the assumption that peaks and valleys independently follow a Gamma distribution. However, GAMLSS slightly reduces the prediction error of $\sigma.Rpm$ and $\sigma.Rvm$ arising better prediction performance. In contrast, the DRF models achieved higher accuracy in surface roughness prediction. This model surpasses the prediction accuracy of GAMLSS, resulting in the lowest error in terms of RMSE for all predicted variables (see Fig. 11).

Both GAMLSS and DRF are feasible solutions to represent the cylindrical grinding process. Notwithstanding, each of these models has advantages over the other. For example, DRF predicts all the characteristics of the roughness profile with better accuracy, but explaining the relationship between the response variables and their predictors is complex due to its fitting nature as a group of distributional trees. On the other hand, in GAMLSS models, its accuracy might be slighter than DRF, but instead, its interpretability is the highest thanks to the additive polynomial relations between inputs and outputs, which effectively facilitate the creation of optimal working windows.

With the DRF models, two conditions were predicted to illustrate the response of this approach and explain the differences between the different coolant/lubricant systems. Figure 12 shows the distributions of surface roughness

profiles for the ground condition: *Vs*=52.6 m/s, *Vo*=13.82 m/min, and *GroundVol*=0 mm^3. Also, this figure shows the experimental and predicted values for *Rpm*, σ.*Rpm*, *Rvm*, σ.*Rvm*, *Ra*, and σ.*Ra*. Additionally, the feature importances of the Random Forest models can be explored, which provide insights into the key factors influencing the predictions, similar to the approach used in the GAMLSS model.

In this figure, several comparisons can be achieved. For example, the distribution in pink shows the surface roughness profile for the experimental condition, in which the LN_2 was used as the cooling system. By comparing this distribution with the distribution in cyan, that is, the predicted condition for LN_2, it is possible to validate the model's accuracy with a 6.24% in *Ra* and 1.92% for σ.*Ra*.

Additionally, in Fig. 12, it is possible to compare the LN_2 approach with the WET and LN_2+MQL approaches. For this condition, with GroundVol equal to 0 mm^3, which means the grinding wheel was just dressed, the differences between the three coolant/lubricant approaches are evident. WET predicted surface roughness distribution shows a decrease of 12.04% in *Ra* and 9.82% in σ.*Ra* from the predicted LN_2 values. However, the LN_2+MQL surface shows a higher decrease of 23.60% in *Ra* and 24.52% in σ.*Ra*. Thanks to the ensemble model developed, it is possible to conclude that for the tested condition, the approach that produces less surface roughness in terms of mean and variance is the LN_2 +MQL. As this example shows, the model can be a practical instrument to predict and reduce the surface roughness of the ground surfaces by discovering the correct machining condition based on the cryogenic system utilized.

To analyze the grinding wheel performance over the cryogenic approaches, Fig. 13 shows the distributions of surface roughness profiles for the ground condition: *Vs*=52.6 m/s, *Vo*=13.82 m/min, and *GroundVol*=2016 mm^3. In this grinding condition, the wheel present wear and dullness for all coolant/lubricant approaches, evidenced by Fig. 8. Furthermore, Fig. 13 details the experimental and predicted values for all surface indicators studied. In this figure, the distribution in pink is the response of the LN_2+MQL approach. By comparing this plot with the distribution in purple, the relative error for *Ra* and σ.*Ra* is 2.72% and 5.01%, respectively. In this way, it is possible to validate the model's accuracy for predicting surface roughness, including in the analysis of the wheel performance, which is vital for process industrialization.

In Fig. 13, it is also possible to appreciate the comparison of the three coolant/lubricant approaches. Curiosity, the mean surface roughness, and the global dispersion of the profile exposed different behavior. Minimum differences were found in *Ra* with values of 0.36% for WET and 0.33% for LN_2 over LN_2+MQL. In the case of the global dispersion σ.*Ra*, WET approach increases the dispersion with a

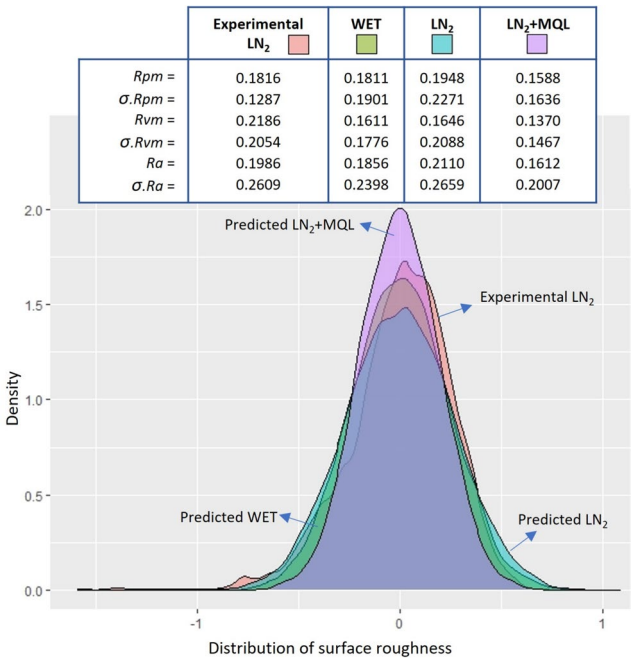

Fig. 12 Predicted surface roughness profile for the machining condition: *Vs*=52.6 m/s, *Vo*=13.82 m/min, and *GroundVol*=0 mm^3 under all coolant/lubricant systems. Additionally, the experimental surface roughness profile when using LN_2 under the same machining condition is present for comparison

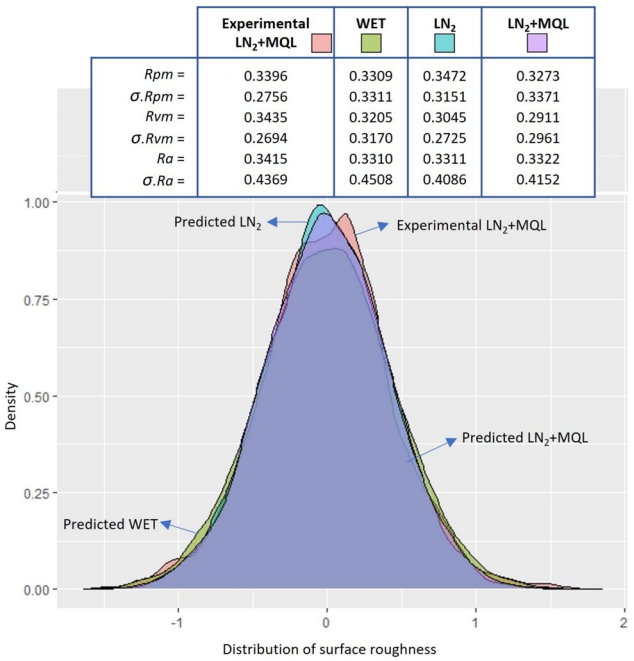

Fig. 13 Predicted surface roughness profile for the machining condition: *Vs*=52.6 m/s, *Vo*=13.82 m/min, and *GroundVol*=2016 mm^3 under all coolant/lubricant systems. Additionally, the experimental surface roughness profile when using LN_2+MQL is present for comparison

predicted increase of 8.57% over LN_2+MQL. In contrast, LN_2 decrees $\sigma.Ra$ with a predicted value of 1.59% over LN_2+MQL. These results show evidence to conclude that the grinding wheel's performance might not be affected by the use of cryogenic approaches. Moreover, cryogenic approaches produce slender surface roughness profiles than WET when the wheel accumulates wear and dullness.

To analyze the interpretability of GAMLSS models, Figs. 14 and 15 represent the visual analysis of the peaks and valleys models. These figures show the direct partial effect of the explanatory variables over the predicted means (*Rpm* and *Rvm*) and their standard deviations ($\sigma.Rpm$ and $\sigma.Rvm$). For example, Fig. 14a reveals that the grinding wheel speed shows a quadratic relationship with a minimum value in *Vs*=52.6 m/s. Then, the effect over *Rpm* is positive for lower or higher speeds, increasing *Rpm*.

Figure 14b shows the linear behavior of workpiece speed over *Rpm*. For lower workpiece speeds (*Vo*=15 m/min), the speed negatively affects *Rpm*, decreasing the surface roughness. However, for higher speeds (*Vo*=40m/min), the effect is positive, increasing the mean of peaks.

In the case of cooling type, this categorical variable catches the effect of the cooling/lubricant system over *Rpm*. LN_2 and WET slightly increase the mean of peaks. However, in the case of LN_2+MQL, the partial effect is negative, decreasing *Rpm*. This decrease seems to be due to the high lubricant effect of the MQL.

The last parameter is the accumulative ground volume of the grinding wheel (*GroundVol*). This variable represents the performance of the grinding wheel, taking into account the possible wear or dullness of the wheel surface as a consequence of the usual grain wear and the cooling system used in the process. Figure 14d shows the quadratic effect of this variable, in which it is clear to see the tendency that when the *GroundVol* increases, the *Rpm* increases too. For example, after dressing the grinding wheel, where the wear is zero, the effect is negative, reducing *Rpm*. However, after ground 2000 mm^3, the effect changed to positive, increasing the mean roughness of peaks.

By comparing Figs. 14a-d and 15a-d. It is possible to appreciate that the behavior and tendency of explanatory variables over *Rpm* and *Rvm* seem identical. However, by comparing Eq. 13 with Eq. 15, slight differences can be appreciated in the coefficients of the models that produce minimal variation between *Rpm* and *Rvm*.

The fundamental changes in the distribution of peaks and valleys seem to stand out in the dispersion of the profiles. Figures 14e-g and 15e-g show the effects of machining conditions and cooling system over $\sigma.Rpm$ and $\sigma.Rvm$. Comparing these figures, it is possible to notice that the behavior and tendency are entirely different. For instance, in the case of peaks distribution, the effects of the explanatory variables

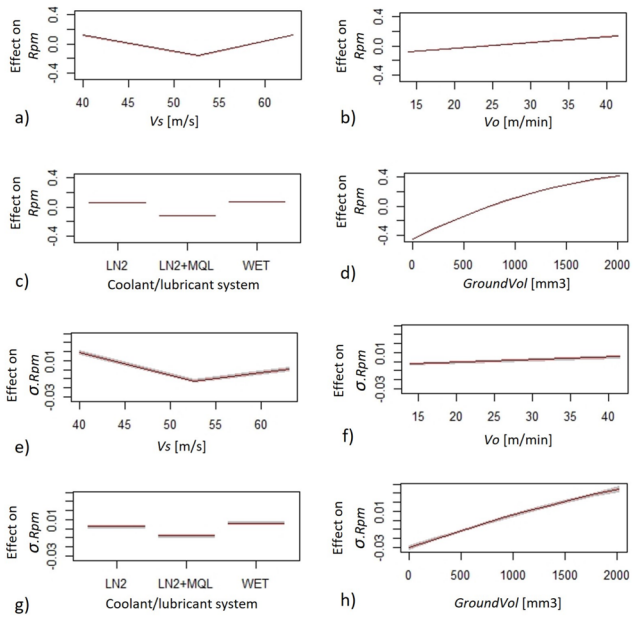

Fig. 14 Explanatory variables effects over *Rpm* (from a to d) and $\sigma.Rpm$ (from e to g) for the GAMLSS peaks model

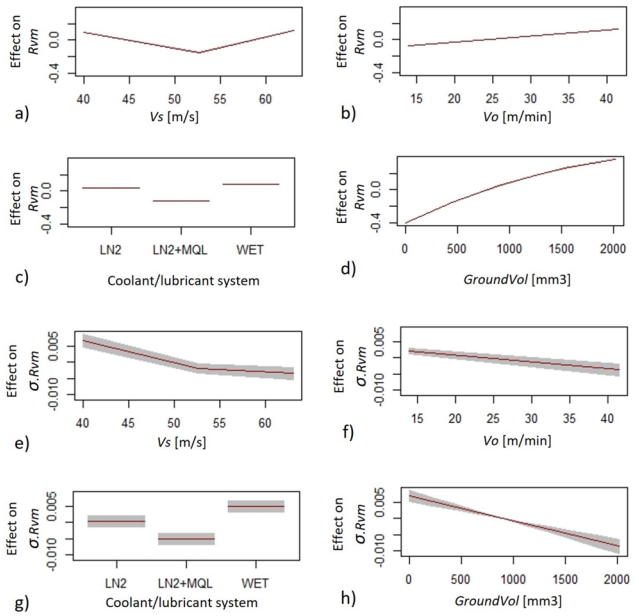

Fig. 15 Explanatory variables effects over *Rvm* (from a to d) and $\sigma.Rvm$ for the GAMLSS Valleys model

over $\sigma.Rpm$ presents a similar trend compared to the effects over *Rpm*, except for two remarks: 1) Effects over $\sigma.Rpm$ varies in the range of ± 0.03 compared to *Rpm* effects for all explanatory variables, and 2) The *GroundVol* variable described in Fig. 14g presents a slight linearization compared to Fig. 14d.

Several differences were found in the case of valleys behavior between *Rvm* and $\sigma.Rvm$. Figure 15e shows the effect of wheel speed over $\sigma.Rvm$. This deviation in the

distribution of valleys increases as a consequence of applying low wheel speeds (*Vs*=40 m/s), and the effect is the opposite for higher speeds (*Vs*=63 m/s), in which the dispersion decreases. Additionally, the workpiece speed effect has an opposite trend for *Rvm* compared to $\sigma.Rvm$. The effect of the workpiece speed over $\sigma.Rvm$ is linear with a negative slope. Therefore, lower speeds (*Vo*=15 m/min) increase $\sigma.Rvm$, and higher speeds (*Vo*=40 m/min) decrease the valleys' dispersion.

The coolant/lubricant systems' effect over the dispersion of valleys is the only variable that presents the same trend as *Rvm*. WET and LN_2 slightly increase the standard deviation, and LN_2+MQL decreases the deviation.

By analyzing the accumulative ground volume of the grinding wheel (*GroundVol*) in Fig. 15h, the trend and behavior of this effect over $\sigma.Rvm$ is different from the rest. The dispersion of valleys decreases when *GroundVol* increases. However, this behavior strengthens the idea that the wear of grains and dullness of the grinding wheel produce a smoother contact surface, generating more homogeneous valleys on the ground surface.

Predicting the surface roughness of a machined piece is essential due to its relation to fatigue behavior that directly affects the mechanical components' life. Several authors have correlated *Ra*, *Rpm*, and *Rvm* with the fatigue life [51, 52]. Thanks to this work, it is possible to predict the key features of the surface roughness profile more accurately and, therefore, select the best process conditions that lead to increased fatigue strength.

Furthermore, the capability of these advanced distributional models extends beyond the cryogenic and wet conditions tested here; they hold significant potential for modeling dry friction processes. As demonstrated by Li et al. [53], dry sliding of eutectoid steels involves complex transitions between mild and severe wear, characterized by high surface temperature fluctuations and microstructural instabilities. These physical phenomena introduce significant stochasticity and heteroscedasticity into the surface roughness profile—characteristics that traditional mean-based regression models often fail to capture. By predicting the full probability distribution (shape and scale parameters) rather than a single point estimate, our distributional ensemble approach is uniquely suited to quantify the high variability and risk associated with dry friction regimes described in [53].

4 Conclusions

The research conducted has a groundbreaking method for predicting surface roughness profile distribution by implementing distributional ensemble modeling, in which peaks and valleys were modeled independently. As a result of this method, new characteristics were identified in the surface roughness of cryogenic ground surfaces utilizing LN_2 and LN_2+MQL. Among the main key characteristics found, the following conclusions can be highlighted:

- We developed a novel distributional ensemble model that, for the first time, independently characterizes the probability distributions of a surface profile's peaks and valleys. This approach provides a far richer and more granular analysis than traditional methods that rely on a single average roughness metric like *Ra*.
- The grinding wheel speed and workpiece speed play a crucial role in determining the effectiveness of cryogenic grinding techniques (LN_2 and LN_2+MQL). The data indicates that if similar surface roughness profiles are desired, it is necessary to adjust the machining conditions when transitioning from flood WET grinding to cryogenic grinding. By accounting for these critical parameters, optimizing the performance of cryogenic grinding processes may be possible.
- By modeling the distribution of the roughness profile, it was possible to identify that cryogenic grinding (LN_2 and LN_2+MQL) shows better performance with lower spindle speed (*Vs*=40 m/s) and workpiece speed (*Vo*=13.82 m/min), since these machining conditions generates surface roughness profiles with similar *Ra* but lower dispersions. This tendency is the opposite of traditional WET flood grinding, which presented similar *Ra* but with higher dispersions of the roughness profile at higher speeds (*Vs*=63 m/s and *Vo*=41.47 m/min).
- GAMLSS and DRF models are feasible solutions to predict surface roughness indicators. DRF models achieve more accuracy than GAMLSS with improvements in RMSE of 11% for *Rpm*, 24% for *Rvm*, 17% for *Ra*, 7% for $\sigma.Rpm$, 8% fo $\sigma.Rvm$, and 17% for $\sigma.Ra$. However, GAMLSS are fully explainable models for peaks and valleys that allow an understanding of the relations between machining conditions and coolant/lubricant system over surface roughness, resulting helpfully in creating optimal process windows.
- The ensemble predictive approach described in this work offers a highly accurate way to predict the dispersion of surface roughness profiles. With an RMSE of 0.071 for *Ra* and 0.066 for $\sigma.Ra$, this approach is beneficial for analyzing the impact of wheel performance while also taking into account the effects of grain wear and dullness that can occur with the use of cryogenic coolant/lubricant approaches in comparison to conventional WET grinding.

Funding This work was supported by the project FATECO [GA:847284, 2018, Research Fund for Coal & Steel].

Declarations

Competing interests The authors declare that they have no known competing financial interests or personal relationships that could have appeared to influence the work reported in this paper. All authors have read and agreed to the published version of the manuscript.

References

1. Khan MA Jaffery SHI, Khan, M. (2023) Assessment of sustainability of machining ti-6al-4v under cryogenic condition using energy map approach. Eng Sci Technol Int J 41:101357. https://www.sciencedirect.com/science/article/pii/S2215098623000344, https://doi.org/10.1016/j.jestch.2023.101357
2. Abedrabbo F, Soriano D, Madariaga A, Fernández R, Abolghasem S, Arrazola PJ (2021) Experimental evaluation and surface integrity analysis of cryogenic coolants approaches in the cylindrical plunge grinding. Sci Rep 11:1–14. https://doi.org/10.1038/s41598-021-00225-6
3. Kishore K, Sinha M, Singh A, Roy A, Gupta M, Korkmaz ME (2022) A comprehensive review on the grinding process: Advancements, applications and challenges. In: Proceedings of the Institution of Mechanical Engineers, Part C: Journal of Mechanical Engineering Science 236:095440622211107. https://doi.org/10.1177/09544062221110782
4. Chattopadhyay AB, Bose A, Chattopdhyay AK (1985) Improvements in grinding steels by cryogenic cooling. Precision Eng 7:93–98. https://doi.org/10.1016/0141-6359(85)90098-4
5. Paul S, Bandyopadhyay PP, Chattopadhyay AB (1993) Effects of cryo-cooling in grinding steels. J Mater Process Tech 37:791–800. https://doi.org/10.1016/0924-0136(93)90137-U
6. Paul S, Chattopadhyay AB (1995) Effects of cryogenic cooling by liquid nitrogen jet on forces, temperature and surface residual stresses in grinding steels. Cryogenics 35:515–523. https://doi.org/10.1016/0011-2275(95)98219-Q
7. Bhaduri D, Kumar R, Chattopadhyay AK (2011) On the grindability of low-carbon steel under dry, cryogenic and neat oil environments with monolayer brazed cBN and alumina wheels. Int J Adv Manufact Technol 57:927–943. https://doi.org/10.1007/s00170-011-3341-3
8. Manimaran G, Pradeep Kumar M (2013) Effect of cryogenic cooling and sol-gel alumina wheel on grinding performance of AISI 316 stainless steel. Arch Civil Mech Eng 13:304–312. https://doi.org/10.1016/j.acme.2013.03.002
9. Balan AS, Chidambaram K, Kumar AV, Krishnaswamy H, Pimenov DY, Giasin K, Nadolny K (2021) Effect of cryogenic grinding on fatigue life of additively manufactured maraging steel. Materials 14:1–16. https://doi.org/10.3390/ma14051245
10. Gong Y, Xu J, Buchanan RC (1998) A Neural Network Process Model for Abrasive Flow Machining Operations. J Manufact Syst 17:52–64. https://doi.org/10.1016/S0278-6125(98)80009-5
11. Viharos ZJ (1999) A general ANN model of turning and its application for surface roughness estimation using acoustic emission signal. MOSYCUT Workshop-Ljubljana 1–6
12. Arapoğlu RA, Sofuoğlu MA, Orak S (2017) An ANN-Based Method to Predict Surface Roughness in Turning Operations. Arabian J Sci Eng 42:1929–1940. https://doi.org/10.1007/s13369-016-2385-y
13. Kaufmann T, Sahay S, Niemietz P, Trauth D, Maas W, Bergs T (2020) AI-based Framework for Deep Learning Applications in Grinding. In: SAMI 2020 - IEEE 18th world symposium on applied machine intelligence and informatics, proceedings, pp 195–200. https://doi.org/10.1109/SAMI48414.2020.9108743
14. Pan Y, Wang Y, Zhou P, Yan Y, Guo D (2020) Activation functions selection for bp neural network model of ground surface roughness. J Intell Manufact 31:1825–1836. https://doi.org/10.1007/s10845-020-01538-5
15. Hadad M, Attarsharghi S, Dehghanpour Abyaneh M, Narimani P, Makarian J, Saberi A, Alinaghizadeh A (2024) Exploring new parameters to advance surface roughness prediction in grinding processes for the enhancement of automated machining. J Manufact Mater Process 8:41
16. Uçar F, Katı N (2020) Machine learning based predictive model for surface roughness in cylindrical grinding of al based metal matrix composite. Eur J Technique (EJT) 10:415–430
17. Malakooti BB, Zhou YQ, Tandler EC (1995) In-process regressions and adaptive multicriteria neural networks for monitoring and supervising machining operations. J Intell Manufact 6:53–66. https://doi.org/10.1007/BF00123676
18. Wang J, Tian Y, Hu X, Fan Z, Han J, Liu Y (2024) Development of grinding intelligent monitoring and big data-driven decision making expert system towards high efficiency and low energy consumption: experimental approach. J Intell Manufact 35:1013–1035. https://doi.org/10.1007/s10845-023-02089-1
19. Thankachan T, Soorya Prakash K, Malini R, Ramu S, Sundararaj P, Rajandran S, Rammasamy D, Jothi S (2019) Prediction of surface roughness and material removal rate in wire electrical discharge machining on aluminum based alloys/composites using Taguchi coupled Grey Relational Analysis and Artificial Neural Networks. Appl Surface Sci 472:22–35. https://doi.org/10.1016/j.apsusc.2018.06.117
20. Park SH, Park KS (2023) A pre-trained model selection for transfer learning of remaining useful life prediction of grinding wheel. J Intell Manufact. https://doi.org/10.1007/s10845-023-02154-9
21. Outeiro JC (2014) Surface integrity predictions and optimisation of machining conditions in the turning of AISI H13 tool steel. Int J Machining Machinability Mater 15:122–134. https://doi.org/10.1504/IJMMM.2014.059189
22. Agrawal A, Choudhary A (2018) An online tool for predicting fatigue strength of steel alloys based on ensemble data mining. Int J Fatigue 113:389–400. https://doi.org/10.1016/j.ijfatigue.2018.04.017
23. Zhang W, Bao Z, Jiang S, He J (2016) An artificial neural network-based algorithm for evaluation of fatigue crack propagation considering nonlinear damage accumulation. Materials 9. https://doi.org/10.3390/ma9060483
24. Vrabel M, Mankova I, Beno J, Tuharský J (2012) Surface roughness prediction using artificial neural networks when drilling UDIMET 720. Procedia Engineering 48:693–700. https://doi.org/10.1016/j.proeng.2012.09.572
25. Cerutti, F., Srivastava, M., Preece, A., Julier, S., Rao, R.M., Kelley, T.D., Braines, D., Sensoy, M., Willis, C.J., Gurram, P., 2017y.

Interpretability of Deep Learning Models : A Survey of Results. 2017 IEEE SmartWorld, Ubiquitous Intelligence Computing, Advanced Trusted Computed, Scalable Computing Communications, Cloud Big Data Computing, Internet of People and Smart City Innovation (SmartWorld/SCALCOM/UIC/ATC/CBDCom/IOP/SCI) , 1–6https://doi.org/10.1109/UIC-ATC.2017.8397411.
26. Geman S, Bienenstock E, Doursat R (1992) Neural Networks and the Bias/Variance Dilemma. Neural Comput 4:1–58. https://doi.org/10.1162/neco.1992.4.1.1
27. Pandiyan V, Caesarendra W, Tjahjowidodo T, Tan HH (2018) In-process tool condition monitoring in compliant abrasive belt grinding process using support vector machine and genetic algorithm. J Manufact Processes 31:199–213. https://doi.org/10.1016/j.jmapro.2017.11.014
28. Son NH, Trung DD, Nguyen, NT (2020) Surface roughness prediction in grinding process of the SKD11 steel by using response surface method. In: IOP Conference series: materials science and engineering 758:012029. https://doi.org/10.1088/1757-899x/758/1/012029
29. Kim YM, Shin SJ, Cho HW (2022) Predictive Modeling for Machining Power Based on Multi-source Transfer Learning in Metal Cutting. Int J Precision Eng Manufact - Green Technol 9:107–125. https://doi.org/10.1007/s40684-021-00327-6
30. Pandiyan V, Caesarendra W, Glowacz A, Tjahjowidodo T (2020) Modelling of material removal in abrasive belt grinding process: A regression approach. Symmetry 12. https://doi.org/10.3390/SYM12010099
31. Shanmugasundar G, Vanitha M, Čep R, Kumar V, Kalita K, Ramachandran M (2021) A comparative study of linear, random forest and adaboost regressions for modeling non-traditional machining. Processes 9. https://doi.org/10.3390/pr9112015
32. Sauter E, Sarikaya E, Winter M, Wegener K (2021) In-process detection of grinding burn using machine learning. Int J Adv Manuf Technol 115:2281–2297. https://doi.org/10.1007/s00170-021-06896-9
33. Cho S, Asfour S, Onar A, Kaundinya N (2005) Tool breakage detection using support vector machine learning in a milling process. Int J Mach Tools Manuf 45:241–249. https://doi.org/10.1016/j.ijmachtools.2004.08.016
34. Yao Z, Mei D, Chen Z (2010) On-line chatter detection and identification based on wavelet and support vector machine. J Mater Process Technol 210:713–719. https://doi.org/10.1016/j.jmatprotec.2009.11.007
35. Yang Z, Yu Z (2012) Grinding wheel wear monitoring based on wavelet analysis and support vector machine. Int J Adv Manuf Technol 62:107–121. https://doi.org/10.1007/s00170-011-3797-1
36. Bhushan B (2000) Modern tribology handbook. CRC Press, Columbus, Ohio
37. Rigby R, Stasinopoulos M, Heller G, De Bastiani F (2019) Distributions for Modelling Location. Using GAMLSS in R. CRC Press, Scale and Shape
38. Stasinopoulos MD, Rigby RA, De Bastiani F (2018) GAMLSS: A distributional regression approach. Stat Model 18:248–273. https://doi.org/10.1177/1471082X18759144
39. Schlosser L, Hothorn T, Stauffer R, Zeileis A (2019) Distributional regression forests for probabilistic precipitation forecasting in complex terrain. Ann Appl Stat 13:1564–1589. https://doi.org/10.1214/19-AOAS1247, arXiv:1804.02921
40. Perez I, Madariaga A, Arrazola P, Cuesta M, Soriano D (2021) An analytical approach to calculate stress concentration factors of machined surfaces. Int J Mech Sci 190:106040. https://doi.org/10.1016/j.ijmecsci.2020.106040
41. Murphy KP (2012) Machine Learning: A Probabilistic Perspective. MIT Press, London, England
42. Hardin JW, Hilbe JM (2018) Generalized Linear Models and Extensions, Second Edition. Fourth edi ed., Stata Press
43. Zhao Y (2013) Chapter 5 - regression. In: Zhao Y (Ed.), R and Data Mining. Academic Press, pp. 41–50. https://www.sciencedirect.com/science/article/pii/B9780123969637000052, https://doi.org/10.1016/B978-0-12-396963-7.00005-2
44. Breiman L, Friedman J, Stone CJ, Olshen RA (1984) Classification and Regression Trees. Chapman and Hall/CRC
45. Akaike H (1974) A new look at the statistical model identification. IEEE Trans Autom Control 19:716–723. https://doi.org/10.1109/TAC.1974.1100705
46. Singh PK, Kumar S, Jain PK (2023) Surface integrity of cryogenically finished additively manufactured and conventional ti-6al-4v alloy. Metals 13. https://doi.org/10.3390/met13040693
47. Wang Y, Li XD, Feng Z (1995) The relationship between the product of load and sliding speed with friction temperature and sliding wear of a 52100 steel. Scripta metallurgica et materialia 33
48. Wang Y, Yan M, Li X, Lei T (1994) Frictional temperature field and wear behavior of steel 52100 with different microstructures
49. Daneshi A, Jandaghi N, Tawakoli T (2014) Effect of dressing on internal cylindrical grinding. Procedia CIRP 14:37–41. https://doi.org/10.1016/j.procir.2014.03.064
50. Zhou X, Xi F (2002) Modeling and predicting surface roughness of the grinding process. Int J Mach Tools Manuf 42:969–977. https://doi.org/10.1016/S0890-6955(02)00011-1
51. Javadi H, Jomaa W, Texier D, Brochu M, Bocher P (2017) Surface roughness effects on the fatigue behavior of as-machined inconel718. In: Materials Structure and Micromechanics of Fracture VIII, Trans Tech Publications Ltd. pp 306–309. https://doi.org/10.4028/www.scientific.net/SSP.258.306
52. Arola D, Williams C (2002) Estimating the fatigue stress concentration factor of machined surfaces. Int J Fatigue 24:923–930. https://www.sciencedirect.com/science/article/pii/S0142112302000129, https://doi.org/10.1016/S0142-1123(02)00012-9
53. Xiaodong L, You W, Jiajun L (1991) A study on dry friction of eutectoid steel. Wear 150:59–65